Journal of Alloys and Compounds 654 (2016) 56–62

Contents lists available at ScienceDirect

Journal of Alloys and Compounds

journal homepage: http://www.elsevier.com/locate/jalcom

Characterisation of precipitation upon cooling of an AA2618 Al–Cu–Mg alloy

N. Chobaut [a, *], D. Carron [b], J.-M. Drezet [a]

[a] Ecole Polytechnique Fédérale de Lausanne, Laboratoire de Simulation des Matériaux, Station 12, CH-1015 Lausanne, Switzerland
[b] Univ Bretagne Sud, LIMATB, EA 4250, Rue de St Maudé, F-56100, Lorient, France

ARTICLE INFO

Article history:
Received 23 July 2015
Received in revised form
11 September 2015
Accepted 14 September 2015
Available online 15 September 2015

Keywords:
Aluminum alloys
Precipitation
Resistivity
Calorimetry
Gleeble machine

ABSTRACT

The precipitation of an AA2618 Al–Cu–Mg alloy is monitored during isothermal holdings and continuous coolings. The Time-Temperature-Property and Continuous-Cooling-Precipitation diagrams of AA2618 are obtained using in-situ resistivity and differential scanning calorimetry respectively. The two precipitation domains observed at high temperature and low temperature (<300 °C) are discussed with regard to their influence on the mechanical properties during quenching of large components.

1. Introduction

High strength heat-treatable aluminium alloys (AA) are widely used for engineering applications where high formability, environmental resistance and specific mechanical properties are required. The desired mechanical properties are obtained by a heat treatment in three steps: solution heat treatment (SHT), quenching and artificial ageing. The SHT objective is to obtain a solid solution at equilibrium. The quenching objective is to cool the material to room temperature as fast as possible and have thus a state called supersaturated solid solution, as close as possible to solid solution at the end of the quench. The artificial ageing objective is to transform elements in solid solution into fine hardening precipitates and thus increase the yield strength. This last step features two stages in Al–Cu–Mg-based alloys. In the first stage, the hardness almost doubles within 2 min at 200 °C compared to its as-quenched value as shown by Polmear [1]. Deschamps et al. [2] attributed this rapid hardening to the formation of Cu–Mg-rich clusters according to small-angle X-ray scattering (SAXS) and 3D atom probe tomography measurements. After a plateau during ca. 2 h measured by Lu et al. [3], the hardness increases in the second stage to reach its peak value after ca. 9 h at 200 °C where equilibrium *S* (Al_2CuMg) and metastable *S'* precipitates are found.

While precipitates are formed purposely during artificial ageing, they are not desired in an ideal quench that must be fast enough to obtain a supersaturated solid solution. However, fast quenching cannot be achieved in the centre of large components, where the quenching rate can be more than one order of magnitude lower than at the surface. This results in:

- possible coarse precipitation of the *S*/*S'* phases which is detrimental to the final yield strength since it decreases the hardening potential by pumping solute elements during quenching, and
- usually unwanted residual stresses (RS) that depend on the cooling rate, and on the component size and shape but also, as shown in the case of Al–Zn–Mg–Cu thick cold-water quenched plates [4], on the precipitation that forms during quenching.

These two possible issues motivate the need to characterise precipitation during cooling from the SHT temperature in order to take it into account in the simulation of RS formation during quenching of large components [5].

Continuous cooling precipitation diagrams are useful as they describe the influence of cooling rate on precipitation. For AA, differential scanning calorimetry (DSC) has been established as an

* Corresponding author.
E-mail address: nicolas.chobaut@epfl.ch (N. Chobaut).

http://dx.doi.org/10.1016/j.jallcom.2015.09.113
0925-8388/

appropriate tool to determine such diagrams, see for instance Milkereit et al. [6]. In-situ resistivity measurement is also useful to monitor precipitation phenomena during continuous cooling as shown by Archambault and Godard [7]. They validated this method against DSC experiments and extended it to isothermal quenching (IQ), which consists in quenching the alloy down to a given temperature and holding it at this temperature. The resistivity evolution during IQ was used to calibrate thermodynamic-based precipitation models, see for instance Godard et al. [8]. These models were coupled to FE quenching simulations in the works of Godard et al. [9] and Chobaut [10], in order to improve RS predictions in thick heat treatable AA components in relation to their precipitation state.

In the present work, IQ resistivity measurements are performed to characterise the high temperature precipitation kinetics of an Al–Cu–Mg alloy. Thermo-mechanical Gleeble tests in similar IQ conditions are performed to determine the influence of precipitation on flow stress. Complementary to these isothermal measurements, isochronal DSC cooling experiments are applied at cooling rates close to industrial practice at high temperature to determine the influence of high temperature precipitation on the formation of precipitates at low temperature and derive the continuous cooling precipitation diagram of AA2618 not available in the literature.

2. Experimental procedure

2.1. Material

The investigated Al–Cu–Mg alloy is an industrial AA2618 which is used for turbo chargers impellers which are machined from forgings. Specimens have been taken out of a given forging with uniform chemical composition (given in Table 1).

2.2. Isothermal quenching measurements

A Gleeble 3500 machine was chosen for its precise temperature control in order to perform IQ to characterise the alloy by means of resistivity and tensile tests.

IQ resistivity measurements have been done in the Gleeble using the sample configuration described in Ref. [11], i.e. using copper grips together with a specimen geometry optimised for resistivity measurements. All specimens where solutionised in the Gleeble for at least 15 min at a SHT temperature of 530 °C and then quenched to the desired temperature at a cooling rate around 20 K/s.

Thermo-mechanical Gleeble tests have been carried out using the sample configuration described in Ref. [4], i.e. using copper grips together with the specimen geometry optimised for tensile tests. Specimens were then heated in the Gleeble from room temperature to the SHT temperature at 30 K/s, solutionized for 3 min and cooled down at 20 K/s. The coolings were interrupted at either 450 °C, 400 °C, 350 °C, 300 °C, 250 °C, 200 °C or 150 °C to perform isothermal tensile loads at constant displacement rates. At high temperatures (≥350 °C), different strain-rates and pseudo-relaxations (blocked jaws) were imposed in order to characterise the strain-rate sensitivity. At temperatures lower than 350 °C, high strain-rates (>0.01 s^{-1}) were chosen to limit the effect of precipitation on yield strength during loading. This effect of precipitation on yield strength has been characterised with various waiting times before loading. The measurement method is fully detailed in Ref. [10].

Table 1
Measured chemical composition of the Al–Cu–Mg alloy (in wt.%).

Elements	Si	Fe	Cu	Mn	Mg	Cr	Ni	Zn	Ti	Zr
wt.%	0.2	1.1	2.4	0.01	1.55	0.004	1.1	0.1	0.06	0.001

2.3. Non-isothermal cooling

Precipitation upon cooling has been characterised by DSC with various constant cooling rates. A Netzsch 204F1 Phoenix® heat flow differential scanning calorimeter was used with cylindrical samples (4.5 mm diameter, 1.9 mm thick, ca. 82 mg) placed in standard aluminium crucibles (ca. 39 mg, pierced lid). A high purity aluminium Al4N reference sample was placed in the reference furnace. Measurements were done at ambient pressure and under nitrogen as protective gas. Prior to cooling, in situ solutionising treatment was achieved in the calorimeter at 530 °C for 2 h. Two successive complete thermal cycles were achieved for each sample in order to check reproducibility.

The experimental procedure is based on the works of Milkereit et al. [12,13]. It consists, for each cooling rate, in measuring an instrumental baseline with Al4N samples in reference and sample furnaces and subtracting this instrumental baseline from the heat-flow curve of the corresponding sample measurement. This is followed by the subtraction of the experimental baseline determined by a polynomial fit of the background of the resulting curve. DSC signal being proportional to sample mass and scanning rate, the resulting corrected heat flow curve is normalised by dividing by sample mass and cooling rate. When two peaks overlap the obtained curve, so-called “excess specific heat”, is fitted by two Gaussian functions. The precipitation start and end temperatures are determined from the fit. The area under the peak(s) gives information about the released specific heat called “specific precipitation heat”. This value is a measurement of the volume fraction of precipitates.

In order to complement the DSC results, five Vickers hardness indentations (1 kg for 20 s) were performed on each sample after natural ageing at 20 °C for 24 h followed by artificial ageing at 200 °C for 20 h.

3. Results

3.1. Isothermal quenching

3.1.1. Resistivity measurements

The results of IQ measurements are given in Fig. 1 where the

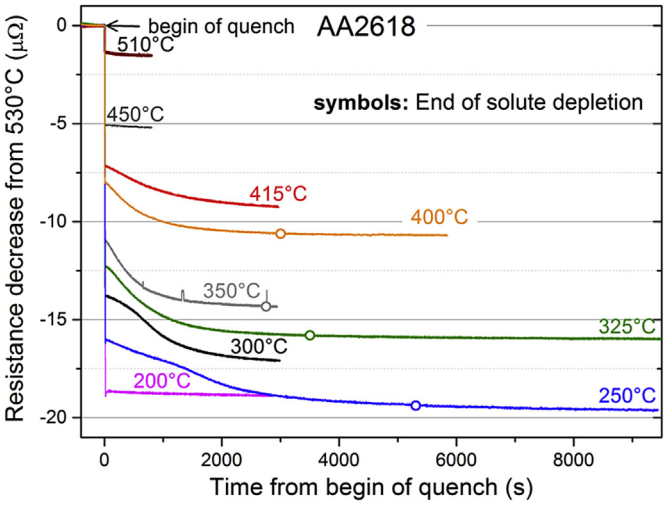

Fig. 1. Evolution of resistance decrease from 530 °C during IQ at different temperatures.

resistance decrease is obtained by subtracting the resistance value at 530 °C from the current resistance value.

In the absence of metallurgical change, the resistance should be constant at a given temperature. This is the case for pure aluminium specimens measured in the Gleeble machine which exhibit a very slight drop of resistance with time (max. 3×10^{-4} $\mu\Omega^{-1}$) [11]. This should be also the case in aluminium alloys at temperatures higher than their solvus. In Fig. 1, the drop of resistance with time in AA2618 is in the order of 10^{-4} $\mu\Omega^{-1}$ (same operating area as for pure aluminium specimens in Ref. [11]) at 510 °C and 450 °C. This is compatible with the drop of resistance measured in pure aluminium and with the solvus predicted by ThermoCalc software for AA2618, 475 °C. The resistance drop value of 10^{-4} $\mu\Omega^{-1}$ is chosen as a criterion to determine the value of the resistance decrease corresponding to a solid solution at equilibrium, R_{end}, indicated by open circles in Fig. 1.

At temperatures ranging from 250 °C to 415 °C, precipitation takes place as it can be seen by the large drop of resistance on isothermals due to solute loss. The criterion chosen to determine R_{end} indicates that solute depletion is maximal after ca. 3000 s at 400 °C, 2800 s at 350 °C, 3500 s at 325 °C and 5300 s at 250 °C. With a final drop of resistance with time of ca. 2×10^{-4} $\mu\Omega^{-1}$ the isothermal holdings at 415 °C and 300 °C were slightly too short to obtain a solid solution at equilibrium. However, this is of second importance for industrial practice where the beginning of solute loss matters most.

Resistivity increase can be usually observed during residual resistivity measurements in liquid nitrogen [14]. This effect is generally suppressed in Al-based alloys at higher measuring temperatures [15,16]. This is the case at 200 °C in Fig. 1 where no significant resistance change is observed during the first 50 min. Other methods such as small angle scattering experiments have been used in the literature to monitor precipitation at low temperature, see for example Deschamps et al. [2].

3.1.2. Tensile tests

The tensile curves at 300 °C and 350 °C are shown in Fig. 2-a and b respectively after various waiting times at these temperatures.

At 300 °C (Fig. 2-a) where strain-rate sensitivity was found to be negligible [10], the flow stress increases from 1 s to 300 s waiting time. This precipitation strengthening at 300 °C was also evidenced at 250 °C, 200 °C and 150 °C for waiting times lower than 200 s [10].

Above 300 °C, no strengthening was observed as shown for instance at 350 °C in Fig. 2-b where the slightly higher flow stress after 60 s than that after 1 s waiting time might be an experimental error or due to the higher strain-rate achieved after 60 s compared to the one achieved after 1 s. Indeed, AA2618 features a positive strain-rate sensitivity at 350 °C in the testing conditions of Fig. 2-b [10]. At 350 °C, the flow stress decreases significantly from 60 s to 600 s. This is attributed to the formation of coarse precipitates which decrease the solute content and therefore reduce solid-solution strengthening. Coarsening of precipitates during further hot deformation was also suggested to be one of the dominant mechanisms - together with dynamic recovery or dynamic recrystallization - responsible for the observed flow softening at temperature over 250 °C in AA2618 [17,18] and in other Al–Cu–Mg alloys [19]. The tensile curves of AA2618 at 400 °C are given in Fig. 3.

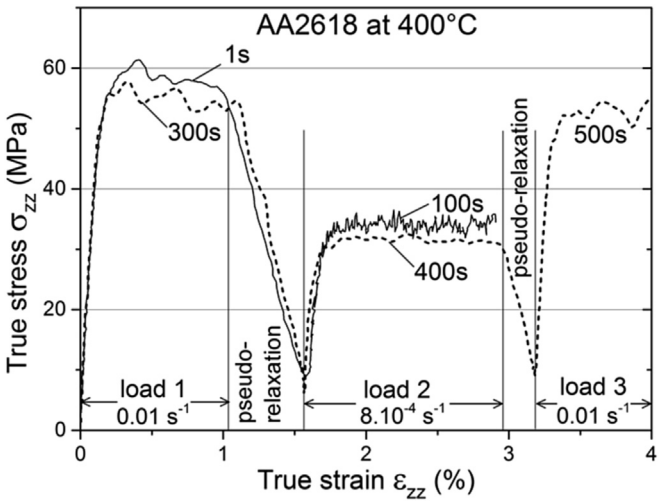

Fig. 3. Tensile curves after various waiting times before loading at 400 °C.

At 400 °C (Fig. 3), AA2618 features no strain-hardening but a maximal strain-rate sensitivity [10] as evidence by the different stress plateaux reached during the first and second loads at different strain-rates. About the same flow stress (56 MPa ± 4 MPa) is reached during loads 1 and load 3 performed at the same strain-rate but after different durations at 400 °C. Therefore at 400 °C, although precipitation was highlighted by resistivity measurements, a softening behaviour is not clearly shown and, if existing, is within the uncertainty of the present measurement on AA2618, ±5 MPa [10]. A similar mechanical behaviour was found at 450 °C [10]. The strengthening and softening behaviours for AA2618 in the 150–450 °C temperature range are summarised in Fig. 4 where the yield strength values are useful to calibrate a yield strength model, see for example [20].

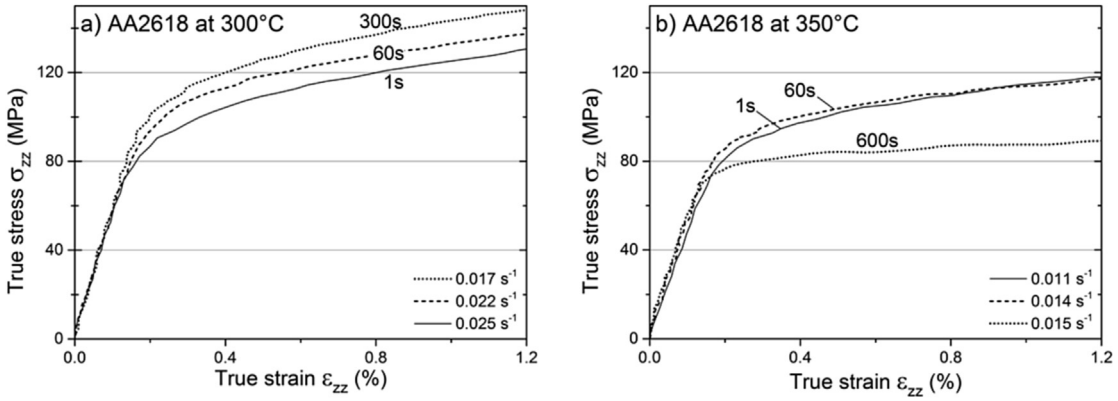

Fig. 2. Tensile curves after various waiting times before loading at 300 °C (a) and 350 °C (b).

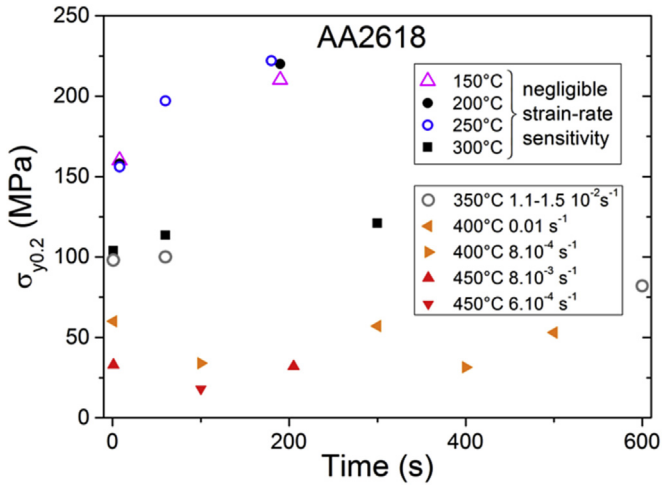

Fig. 4. Yield strength at 0.2% strain offset for AA2618 at different temperatures.

3.2. Non-isothermal cooling

The DSC thermograms achieved with various cooling rates between 1 K/min and 70 K/min are shown in Fig. 5.

For all cooling curves in Fig. 5, two exothermal peaks are observed and the onset of precipitation is detected at ca. 390–410 °C. The high temperature peak increases with decreasing cooling rate down to 1 K/min where two peaks possibly overlap but the signal noise becomes high. The peak split at low cooling rates is due to the precipitation of the S phase or its proposed metastable transitional phases (see next part). The low temperature peak below 300 °C is detected for all cooling rates but with a high signal noise at 1 K/min. The results of hardness measurements complementary to DSC measurements are shown in the next part.

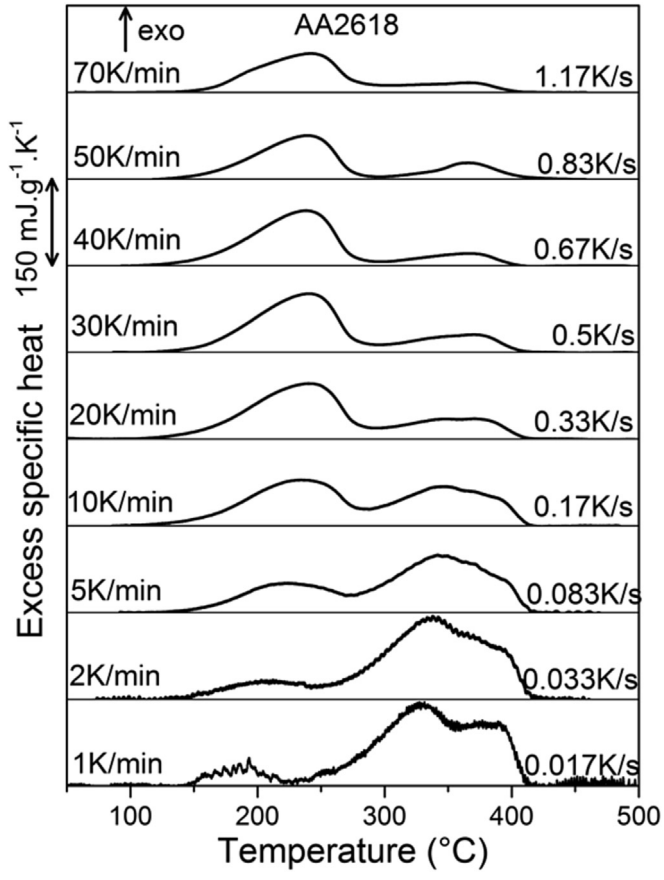

Fig. 5. Selected DSC cooling curves of AA2618 at different cooling rates from 1 to 70 K/min after 2 h solutionising at 530 °C.

4. Discussion

In order to discuss the precipitation kinetics monitored by resistivity, it is convenient to compare the relative resistance decrease ρ, which writes [11]:

$$\rho(T,t) = [R(T,t) - R_{start}(T)]/[R_{end}(T) - R_{start}(T)] \quad (1)$$

where R_{start} is the value of the resistance decrease of the non-equilibrium solid solution and R_{end} is the value of the resistance decrease corresponding to the solid solution at equilibrium. Since R_{end} was not reached experimentally at 300 °C and 415 °C (see Fig. 1), it is estimated by extrapolation of the resistance loss defined as the absolute value of the numerator of ρ. The evolution of the relative resistance decrease is shown in Fig. 6-a. In the Log–log representation of $\rho/(1-\rho)$ versus time given in Fig. 6-b, straight lines are expected if the diffusion-controlled precipitation reaction (of one phase) obeys Austin–Rickett's law [21].

Fig. 6 shows that the fastest precipitation kinetics takes place at 350 °C and the slowest at 250 °C. In Fig. 6-b, apart from short times (<50 s) where measurements are dispersed, straight lines clearly fit experiments at high temperature (≥325 °C). This means that the precipitation reaction above 325 °C obeys Austin–Rickett's law describing one precipitating phase. The slopes, ca. 1.5, are the expected values for diffusion-controlled processes [22]. At lower temperature, however, the curves at 250 °C and 300 °C in Fig. 6-b deviate from straight lines at times corresponding to the first inflection points indicated by the vertical dashed lines in Fig. 6-a. This strongly indicates that more than one phase is precipitating. The Time-Temperature-Property (TTP) diagram of AA2618 is derived from Fig. 6-a by taking the time required to lose 5%, 20%, 50% and 80% of resistance as shown in Fig. 7.

For the TTP-diagram, the experimental data above 300 °C are fitted using C-curves described by Ref. [23]:

$$\tau_C(T) = -k_1 k_2 \exp\left(k_3 k_4^2 \Big/ \left[RT(k_4 - T)^2\right]\right) \exp(k_5/[RT]) \quad (2)$$

where τ_C is the critical time required to precipitate a constant amount of precipitates during the isothermals and k_1 is the natural logarithm of the untransformed fraction. k_2, k_3, k_4 and k_5 are fitting parameters related to the reciprocal of the nucleation site density, the energy required to form a nucleus, the solvus temperature and the activation energy for diffusion respectively. The optimised parameters given in Fig. 7 are in the range of those found in the literature for heat treatable aluminium alloys [24–26]. The fit is acceptable at high temperature, but poor at low temperature (≤300 °C). This is another indication that more than one phase is precipitating below 300 °C.

The mechanical results at 350 °C and 400 °C indicate that the phase forming at these temperatures does not strengthen the material. The fact that the yield strength obtained after 600 s at 350 °C is lower than the initial value at 350 °C can be understood as a decrease of the solid solution contribution to strengthening due to solute loss by large precipitates. This precipitation at such high temperatures is attributed to the formation of the *S* phase or its proposed metastable transitional forms [27] labelled as "*S* (or *S′*)" in Fig. 7 since the distinction between *S* and *S′* (or *S1* and *S2*) as two separate phases is still controversial [28].

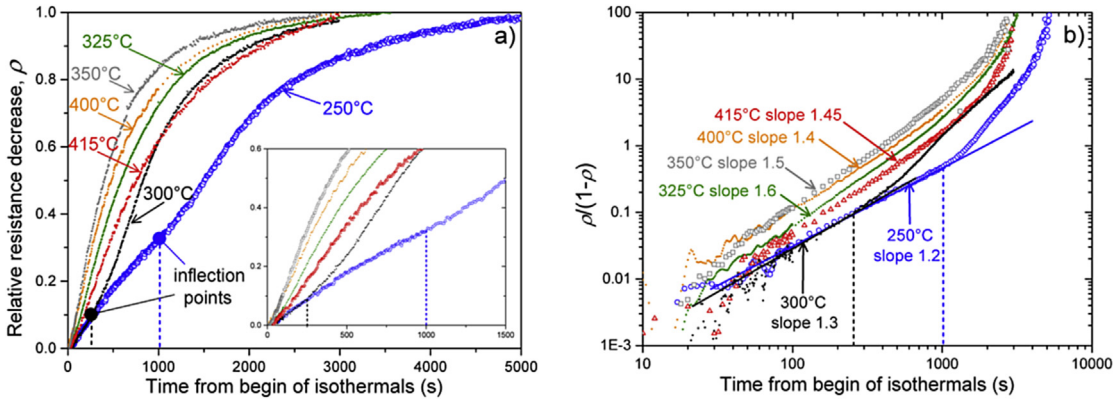

Fig. 6. Normalised precipitation kinetics (a) and log–log representation of ρ/(1−ρ) versus time at various temperatures (b).

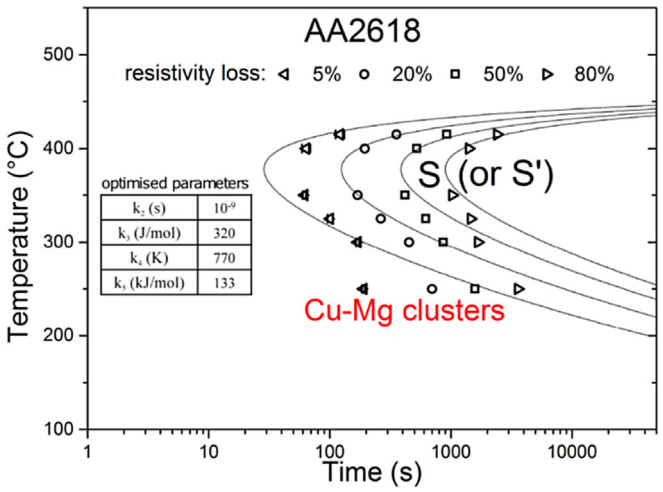

Fig. 7. TTP-diagram of AA2618 obtained by resistivity measurements where C-curves represent iso-resistivity loss and corresponding optimised parameters.

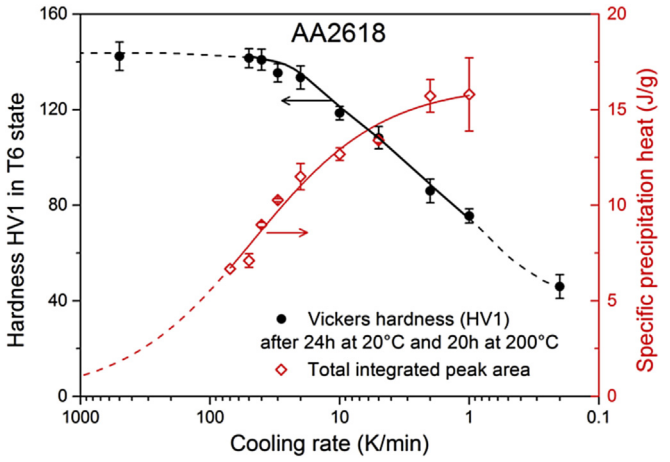

Fig. 8. Vickers hardness and specific precipitation heat of DSC samples after natural ageing at 20 °C for 24 h followed by artificial ageing at 200 °C for 20 h. The hardness and precipitation heat error bars correspond to the standard deviation calculated from at least five indentations and two DSC cycles respectively.

In Fig. 4, the rapid yield strength increase during the first 200 s at 250 °C and during the first 250 s at 300 °C is consistent with the rapid hardening of AA2618 within 2 min at 200 °C attributed to Cu–Mg clusters formation [2]. The first *S*/*S*′ precipitates observed by Deschamps et al. [2] after 20–30 min at 200 °C would explain the hints of possible precipitation of more than one phase at 250 °C and 300 °C after ca. 1000 s and 250 s respectively.

In order to analyse the precipitation kinetics monitored by DSC, the hardness and total specific precipitation heat are shown in Fig. 8 as a function of cooling rate.

The hardness decreases with decreasing cooling rate since the slower the cooling, the higher the solute loss. The T6 hardness values at 0.2 K/min and at ~600 K/min were obtained after cooling in a solutionising furnace (switched-off for slow cooling) and after water quench respectively. The dashed lines are drawn by hand to guide the eye. At high cooling rates (>50 K/min), the dashed line is almost horizontal since Shen [29] measured in AA2618 a slight but not significant T6 hardness increase from 77.5 K/min to 3.8 10^3 K/min.

The total integrated peak area increases with decreasing cooling rate since the slower the cooling, the higher the solute loss by the combined effects of high temperature and low temperature precipitation.

The high temperature precipitation heat (Fig. 9-a) increases with decreasing cooling rate: the slower the cooling, the higher the volume fraction of *S* phase or its proposed metastable transitional forms. The cooling rate at which the high temperature precipitation heat reaches zero is defined as the high temperature critical cooling rate. The higher the high temperature critical cooling rate, the more quench sensitive the alloy. Fig. 9-a shows that the high temperature critical cooling rate of AA2618 is higher than 70 K/min. Although the *S* phase was detected by SAXS at 100 K/s [30], its volume fraction was too low to have a significant effect on the solute content in the matrix. Therefore, the high temperature critical cooling rate of AA2618 is lower than 100 K/s. The extrapolation of the high temperature precipitation heat (dashed line) in Fig. 9-a assuming a sigmoidal shape gives a high temperature critical cooling rate of AA2618 of ca. 1000 K/min (~17 K/s). This value is consistent with the findings of Shen [29] who measured no significant solute loss between 77.5 K/min and 3.8 10^3 K/min.

The low temperature precipitation heat (Fig. 9-b) shows a maximum between 20 and 40 K/min. Cooling slower than 20 K/min leads to large amounts of *S*/*S*′ phases which pump solute that will not be available for precipitation at lower temperatures. Cooling faster than 40 K/min, on the other hand, leads to Cu–Mg cluster formation whose volume fraction decreases with increasing cooling rate owing to longer time available for precipitation. Here, the extrapolation of the low temperature precipitation heat (dashed line in Fig. 9-b) is drawn by hand knowing that the low temperature critical cooling rate of AA2618 is higher than 100 K/s (6.10^3 K/min)

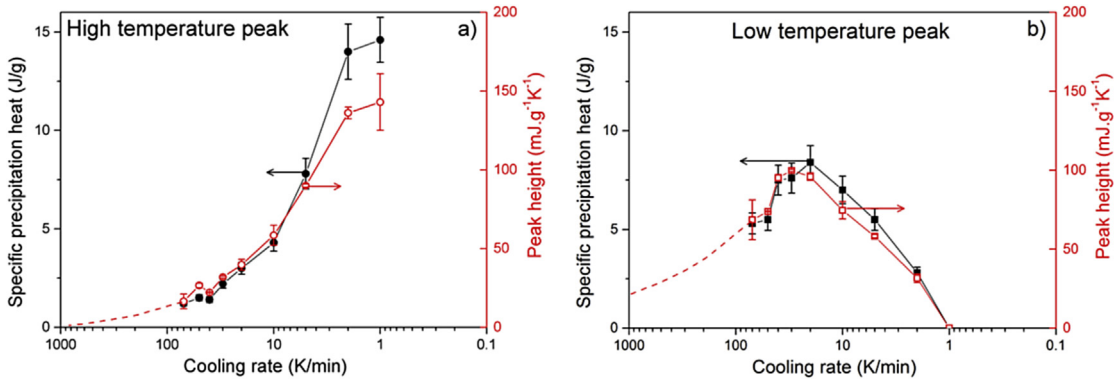

Fig. 9. Specific precipitation heat and peak height of high temperature (a) and lower temperature (b) peaks after cooling of AA2618 at various cooling rates from the SHT temperature.

according to Schloth et al. [30].

The precipitation start and end temperatures determined from the DSC curves are plotted as a function of time in Fig. 10, together with the corresponding cooling curves. Furthermore, three cooling curves achieved in the SAXS measurements by Schloth et al. [30] are superimposed with the corresponding start and end temperatures.

The domain of precipitation of the *S* phase or its proposed metastable transitional forms is indicated schematically in Fig. 10. During fast SAXS cooling, scattering of large objects was detected (open square in Fig. 10) but their volume fraction is difficult to estimate because of anisotropic scattering. The low temperature peak measured by DSC ends at ca. 140–175 °C. Precipitation between ca. 290 °C and 175 °C is attributed to the formation of Cu–Mg cluster [2,30], whose domain is also indicated in Fig. 10. Due to high signal noise at 1 K/min, Cu–Mg cluster formation is considered here to be only evidenced at cooling higher than 2 K/min (0.03 K/s). This precipitation at low temperature cannot be avoided for cooling rates ranging from 0.03 K/s to 100 K/s which are typical of industrial practice. Therefore, the associated strengthening below ca. 300 °C has to be taken into account for accurate residual stress prediction.

5. Conclusions

Precipitation in an Al–Cu–Mg alloy has been characterised during isothermal holdings and continuous coolings by means of resistivity and DSC measurements respectively. The Gleeble machine allowed monitoring the resistance loss in the 250–415 °C temperature range but showed his limitation at 200 °C where no resistance change was detected. Two temperature domains were identified: 325–415 °C where the precipitation reaction obeys Austin–Rickett's law describing one precipitating phase and 250–300 °C where more than one phase is precipitating. Tensile tests in similar precipitation states revealed a softening behaviour at 350 °C and a strengthening behaviour at lower temperatures (≤300 °C). Complementary to these isothermal measurements, DSC measurements at constant cooling rates also revealed two temperature domains consistent with SAXS measurements during coolings close to industrial practice. High temperature precipitation of the stable *S* phase or its proposed metastable transitional forms is highlighted at cooling rates lower than ~17 K/s. Low temperature precipitation of Cu–Mg clusters takes place for cooling rates ranging from 0.03 K/s to 100 K/s. Industrial quenching of large components being within this cooling rate range, precipitation strengthening below ca. 300 °C has to be taken into account for accurate residual stress prediction.

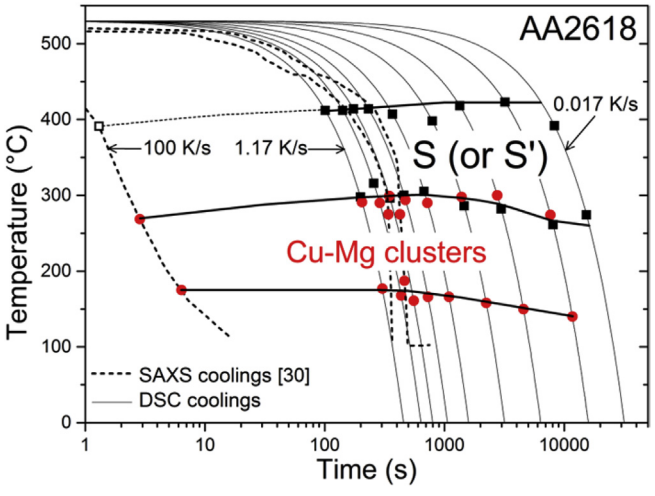

Fig. 10. Continuous cooling precipitation diagram of AA2618 indicating domains where S (or S') and Cu–Mg clusters are detected by DSC or SAXS [30].

Acknowledgement

This work is funded by the Competence Center for Materials Science and Technology (http://www.ccmx.ch/) in the frame of the project entitled "Measurements and modelling of residual stress during quenching of thick heat treatable aluminium components in relation to their microstructure" involving EPF Lausanne, PSI Villigen, Univ. de Bretagne Sud Lorient, Constellium CRV and ABB Turbo Systems Ltd. The Gleeble 3500 machine of Université de Bretagne Sud was co-financed by European Regional Development Fund (ERDF). The authors are grateful to J. Costa (Univ. Bretagne Sud) for the instrumentation of the Gleeble tests, P. Pilvin (Univ. Bretagne Sud) and P. Saelzle (ABB Turbo Systems Ltd.) for fruitful discussion.

References

[1] I.J. Polmear, The effects of small additions of silver on the ageing of some aluminum alloys, Trans. AIME 230 (1964) 1331.
[2] A. Deschamps, T.J. Bastow, F. de Geuser, A.J. Hill, C.R. Hutchinson, In situ evaluation of the microstructure evolution during rapid hardening of an Al–2.5Cu–1.5Mg (wt.%) alloy, Acta Mater. 59 (2011) 2918–2927.
[3] H. Lu, P. Kadolkar, K. Nakazawa, T. Ando, C.A. Blue, Precipitation behavior of AA2618, Metall. Mater. Trans. A 38 (2007) 2379–2388.
[4] N. Chobaut, D. Carron, S. Arsène, P. Schloth, J.M. Drezet, Quench induced residual stress prediction in heat treatable 7xxx aluminium alloy thick plates using Gleeble interrupted quench tests, J. Mater. Process. Technol. 222 (2015) 373–380.
[5] N. Chobaut, P. Saelzle, G. Michel, D. Carron, J.-M. Drezet, Quench-induced

stresses in AA2618 forgings for impellers: a multiphysics and multiscale problem, JOM 67 (2015) 984–990.
[6] B. Milkereit, N. Wanderka, C. Schick, O. Kessler, Continuous cooling precipitation diagrams of Al–Mg–Si alloys, Mater. Sci. Eng. A 550 (2012) 87–96.
[7] P. Archambault, D. Godard, High temperature precipitation kinetics and TTT curve of a 7xxx alloy by in-situ electrical resistivity measurements and differential calorimetry, Scr. Mater. 42 (2000) 675–680.
[8] D. Godard, E. Gautier, P. Archambault, C. Sigli, The modelling of heterogeneous precipitation in Al–Zn–Mg–Cu alloys during quenching, in: Proceedings of the International Conference on Solid-solid Phase Transformations, 1999, pp. 145–148.
[9] D. Godard, P. Archambault, S. Denis, E. Gautier, F. Heymes, Modelling of heat treatment residual stresses. Application to high strength aluminium alloys including precipitation effects, in: J. Lendvai, T. Réti (Eds.), Proceedings of the 7th International Seminar of IFHT on Heat Treatment and Surface Engineering of Light Alloys, 1999, pp. 249–257.
[10] N. Chobaut, Measurements and Modelling of Residual Stresses during Quenching of Thick Heat Treatable Aluminium Components in Relation to their Precipitation State, PhD thesis no 6559 EPFL, 2015, http://dx.doi.org/10.5075/epfl-thesis-6559.
[11] N. Chobaut, D. Carron, J.M. Drezet, Monitoring precipitation kinetics in heat treatable aluminium alloys using in-situ resistivity in Gleeble thermo-mechanical simulator, Mater. Sci. Forum 794–796 (2014) 921–925.
[12] B. Milkereit, O. Kessler, C. Schick, Recording of continuous cooling precipitation diagrams of aluminium alloys, Thermochim. Acta (2009) 73–78.
[13] B. Milkereit, M. Beck, M. Reich, O. Kessler, C. Schick, Precipitation kinetics of an aluminium alloy during Newtonian cooling simulated in a differential scanning calorimeter, Thermochim. Acta 522 (2011) 86–95.
[14] R. Ferragut, A. Somoza, I. Torriani, Pre-precipitation study in the 7012 Al–Zn–Mg–Cu alloy by electrical resistivity, Mater. Sci. Eng. A 334 (2002) 1–5.
[15] I. Kovaćs, J. Lendvai, E. Nagy, The mechanism of clustering in supersaturated solid solutions of A1–Mg_2Si alloys, Acta Metall. 20 (1972) 975–983.
[16] C. Panseri, T. Federighi, Evidence for the interaction between Mg atoms and vacancies in Al–Zn 10%–Mg 0.1% alloy, Acta Metall. 11 (1963) 575–584.
[17] F. Bardi, M. Cabibbo, S. Spigarelli, An analysis of thermo-mechanical treatments of a 2618 aluminium alloy: study of optimum conditions for warm forging, Mater. Sci. Eng. A 334 (2002) 87–95.
[18] P. Cavaliere, Hot and warm forming of 2618 aluminium alloy, J. Light Metals 2 (2002) 247–252.
[19] X.Y. Liu, Q.L. Pan, Y.B. He, W.B. Li, W.J. Liang, Z.M. Yin, Flow behavior and microstructural evolution of Al–Cu–Mg–Ag alloy during hot compression deformation, Mater. Sci. Eng. A 500 (2009) 150–154.
[20] D. Godard, P. Archambault, J.-P. Houin, E. Gautier, F. Heymes, Mechanical softening kinetics at high temperatures in AlMgZnCu alloy: experimental characterization and microstructural interpretation, in: T. Sato, S. Kumai, T. Kobayashi, Y. Murakami (Eds.), Proceedings of ICAA6, 1998, pp. 1033–1038.
[21] L. Eon-Sik, Y.G. Kim, A transformation kinetic model and its application to Cu–Zn–Al shape memory alloys—II. Non-isothermal conditions, Acta Metall. Mater. 38 (1990) 1677–1686.
[22] M.J. Starink, Kinetic equations for diffusion-controlled precipitation reactions, J. Mater. Sci. 32 (1997) 4061–4070.
[23] J.T. Staley, Quench factor analysis of aluminium alloys, Mater. Sci. Technol. 3 (1987) 923–935.
[24] J. Robinson, D. Tanner, S. Van Petegem, A. Evans, Influence of quenching and aging on residual stress in Al–Zn–Mg–Cu alloy 7449, Mater. Sci. Technol. 28 (2012) 420–430.
[25] S. Ma, M.D. Maniruzzaman, D.S. MacKenzie, R.D. Sisson, A methodology to predict the effects of quench rates on mechanical properties of cast aluminum alloys, Metall. Mater. Trans. B 38 (2007) 583–589.
[26] R. Shuey, M. Tiryakioglu, Quenching of aluminium alloys, in: H.M.T.B. Liscic, L.C.F. Canale, G.E. Totten (Eds.), Quenching Theory and Technology, second ed., CRC Press, 2010, pp. 43–83.
[27] M. Styles, C. Hutchinson, Y. Chen, A. Deschamps, T. Bastow, The coexistence of two S (Al 2 CuMg) phases in Al–Cu–Mg alloys, Acta Mater. 60 (2012) 6940–6951.
[28] V. Radmilovic, R. Kilaas, U. Dahmen, G. Shiflet, Structure and morphology of S-phase precipitates in aluminum, Acta mater. 47 (1999) 3987–3997.
[29] P. Shen, The Effects of Heat Treatment on the Microstructure and Mechanical Properties of the AA2618 DC Cast Plate, Master thesis Université du Québec, 2012, ISBN 9781412318761.
[30] P. Schloth, A. Menzel, J.L. Fife, J.N. Wagner, H. Van Swygenhoven, J.M. Drezet, Early cluster formation during rapid cooling of an Al–Cu–Mg alloy: In situ small-angle X-ray scattering, Scr. Mater. ISSN: 1359-6462 x (2015) xx-xx, http://dx.doi.org/10.1016/j.scriptamat.2015.06.015.